Heliyon 10 (2024) e37523

Contents lists available at ScienceDirect

Heliyon

journal homepage: www.cell.com/heliyon

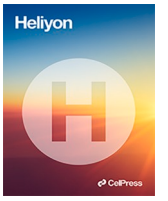

Research article

Chlorogenic acid exhibits antitumor effect in patient-derived xenograft models and hydrogel-embedded tissue culture drug susceptibility test of tongue cancer

Jia Zhu [a,b,c,1], Jiaqi Mei [d,1], Yuanqiao He [e,f], Yan Zou [a,b,c], Xiaoping Hu [a,b,c,*]

[a] The Affiliated Stomatological Hospital, Jiangxi Medical College, Nanchang University, Nanchang, Jiangxi, China
[b] Jiangxi Provincial Key Laboratory of Oral Diseases, Nanchang, Jiangxi, China
[c] Jiangxi Provincial Clinical Research Center for Oral Diseases, Nanchang, Jiangxi, China
[d] Department of Hematology, University Hospitals and University of the Second Clinical Medical College of Nanchang University, Nanchang, Jiangxi, China
[e] Nanchang Royo Biotech Co., Ltd, Nanchang, Jiangxi, China
[f] Center of Laboratory Animal Science, Nanchang University, Nanchang, Jiangxi, China

ARTICLE INFO

Keywords:
Chlorogenic acid
Patient-derived xenograft
Hydrogel-embedded histoculture drug sensitivity test
Tongue cancer

ABSTRACT

Chlorogenic acid (CGA) is one of the effective components of Chinese medicine plant such as honeysuckle and Eucommia ulmoides. CGA can inhibits various cancer types, but its effectivity against tongue cancer remains unknown.

In the present study, we utilized patient-derived xenograft (PDX) models in conjunction with hydrogel-embedded drug sensitivity tests (HDST) to demonstrate the inhibitory effects of CGA on tongue cancer tissues in both in vivo and ex vivo experimental paradigms. Immunohistochemical (IHC) analysis and TUNEL staining revealed that CGA downregulated the expression of CD31 and Ki-67, while concurrently promoting apoptosis. Furthermore, the involvement of the EGFR-AKT-MMP9 signaling cascade in the tumor-suppressive effects of CGA was confirmed using network pharmacology analysis and immunofluorescent validation techniques.

Overall, our findings indicate that CGA robustly inhibits tongue cancer in cellular and organismal models. The EGFR-AKT-MMP9 axis plays a highly significant role in mediating this bioactivity, thereby positioning CGA as a promising candidate for further investigation in oncology. The multifaceted therapeutic potential of CGA, as evidenced by its ability to disrupt angiogenesis, suppress cell proliferation, and induce apoptosis, underscores its value as a novel therapeutic agent for the treatment of tongue cancer.

1. Introduction

Tongue cancer is one of the common types of oral cancer, accounting for 44.1 % of all oral malignancies [1]. The most frequently

* Corresponding author. The Affiliated Stomatological Hospital, Jiangxi Medical College, Nanchang University, Nanchang, Jiangxi, China.
E-mail addresses: 44287374@qq.com (J. Zhu), 2835697176@qq.com (J. Mei), heyuanqiao@ncu.edu.cn (Y. He), 1922988408@qq.com (Y. Zou), 563960724@qq.com (X. Hu).

[1] **Jia Zhu** and **Jiaqi Mei** should be considered joint first author. They contributed equally to this work.

https://doi.org/10.1016/j.heliyon.2024.e37523
Received 8 April 2024; Received in revised form 3 August 2024; Accepted 4 September 2024
Available online 6 September 2024

used treatment for tongue cancer is surgery [2], followed by drug treatment. Currently, chemotherapeutic agents, such as cisplatin and 5-fluorouracil, are used to treat oral cancer after surgery [3]. However, these chemotherapeutic agents are highly toxic to normal cells, often damaging healthy tissues and causing serious adverse effects [4]. The survival rate of tongue cancer is low [5,6], and few anticancer drugs have shown efficacy. A major reason for the numerous failures of clinical trials is the large gap between preclinical models and the treatment situations of patients [7], because the process of generating cancer cell lines results in major and irreversible alterations in biological properties [8]. Therefore, studies have focused on developing and characterizing patient-derived xenografts (PDXs) [9].

PDX models are developed for the study of human tumors implanted in mice. The resulting environments closely resemble the environment of the human body and thus provide valuable information as to how tumors develop and respond to treatment. Hydrogel-embedded histoculture drug sensitivity test (HDST) is a novel drug screening method that uses tumor tissues cultured in laboratories in testing the effectiveness of different drugs and aims to reduce the number of mice used in experiments. Our previous experiment showed that HDST can be used for the rapid, accurate, and economical evaluation of anticancer drugs' preclinical efficacy [10].

Chlorogenic acid (CGA) is widely found in higher dicotyledonous plants, ferns, and many Chinese medicine plants, such as honeysuckle and Eucommia ulmoides, enjoying the reputation of being called "plant gold." It is a polyphenolic compound commonly found in food, such as apples, soy, and coffee [11]. CGA not only has a wide range of pharmacological effects, including antioxidant, antibacterial, antiviral, hypoglycemic, and hypolipidemic [12] but also has a good inhibitory effect on various cancer types, such as lung, liver, and breast cancer, and few side effects in preclinical trial and clinical studies [13–16]. However, its ability to fight tongue cancer has not been reported.

In this article, the effect of CGA on tongue cancer and underlying mechanisms were explored using PDX models and HDST. The results may provide an experimental basis for the clinical application of CGA.

2. Materials and method

2.1. Selection of CGA targets

The three-dimensional structural information of the compound was retrieved from the PubChem database (https://pubchem.ncbi.nlm.nih.gov/). Target proteins of the compound were identified using the Swiss Target Prediction (STP) database (http://www.swisstargetprediction.ch/) with a probability threshold greater than 0. Additionally, the BATMAN-TCM2.0 database (http://bionet.ncpsb.org/batman-tcm/) was utilized to filter target proteins with a cutoff value exceeding 0.85. The resulting target proteins were consolidated by eliminating duplicates to yield a list of potential target proteins for the compound.

2.2. Collection of tongue cancer targets

Genes linked to tongue cancer were identified by searching the term 'tongue cancer' in the DisGeNET (https://www.disgenet.org/), Genecards (https://www.genecards.org/), and OMIM databases (https://omim.org/) with specific filters: a GDA score >0.1 in DisGeNET, a relevance score >10 in Genecards, and relevant gene entries in OMIM. The compiled gene list, after removing duplicates, was intersected with the compound's target proteins to find shared targets.

2.3. Construction of protein-protein interaction

The intersecting target dataset was imported into the STRING database (https://string-db.org/) with *Homo sapiens* selected as the species and a minimum required interaction score set to 0.4. The 'string_interactions_short.tsv' file was then downloaded and imported into Cytoscape 3.7.2 for network visualization. Network topology analysis was conducted using the CytoNCA plugin.

2.4. Construction of drug-compound-target network diagram

The intersection of disease targets and compound targets identified a set of genes potentially responsible for the therapeutic effects. Data corresponding to these genes were extracted from the drug database and compiled into a network, which was then saved as 'network.xlsx'. Subsequently, this network data file was imported into Cytoscape 3.7.2 to visualize the network.

2.5. Patient and tissue samples

Patients' tissue samples were collected under the approval of the ethical committee of the Affiliated Stomatological Hospital of Nanchang University (Permit No. 2021016). The first patient (No. 1) was a 42-year-old male with a pathologist's diagnosis of grade II squamous cell carcinoma of tongue. The second patient (No. 2) was a 57-year-old male with a clinical diagnosis of recurrent medium- and low-differentiated squamous carcinoma of the tongue.

2.6. Materials

Balb/c nude mice aged 6–8 weeks (GemPharmatech Co., Ltd., Jiangsu, China) were used for PDX model establishment and treatment. They were reared in a specific pathogen-free environment. CGA was purchased from Bidepharm (Shanghai, China).

Cisplatin was obtained from Haosen Pharmaceutical Co., Ltd. (Jiangxi, China). All animal studies were approved by the Institutional Animal Care and Use Committee (IACUC) of Royo Biotech Co., Ltd. (RYE: 2020021701, Nanchang, China).

2.7. Establishment of a PDX model

Fresh, active tumor tissues were obtained from each patient and transferred within 4 h under aseptic conditions at low temperatures (2–8 °C). The initially inoculated mice were numbered as P0. When the tissues developed tumors, tumor size was measured using a vernier caliper, and tumor volume (mm^3) was calculated using the following formula: $V = a \times b^2/2$, where V represents the tumor volume and a and b are the largest and smallest tumor diameters, respectively. When the tumor volume exceeded 1000 mm^3, successive generations were passed from P1 generation to P5 generation in mice by using the same method, and P5 mice were used for subsequent experimental studies.

2.8. Hematoxylin–eosin (H&E) staining

Tumor tissues from patients and PDX models were fixed in formalin, embedded in paraffin, prepared into dry 4 μm-thick slides, and stained with hematoxylin–eosin (H&E) with an automatic slide stainer (DP360; DAKEWE, Guangdong, China). Major organs, including the heart, liver, spleen, lung, and kidney, were collected and fixed in formaldehyde for histopathological assessment.

2.9. Immunohistochemistry (IHC)

Immunohistochemistry (IHC) staining was performed using CKpan (ZSGB-BIO, Beijing, China), P40 (ZSGB-BIO), Ki-67 (ZSGB-BIO), and CD31 (ZSGB-BIO) antibodies. The formalin-fixed paraffin-embedded sections of the tissue specimens (thickness, 4 μm) were then stained using a BenchMark XT platform (Roche, Basel, Switzerland) according to the manufacturer's instructions.

2.10. Polymerase chain reaction (PCR)

RNA was extracted on mice from PDX tumor tissues. Primer Premier 5.0 design was used to design human- or mouse-derived genome-specific primers [17]. Extracted samples were amplified by polymerase chain reaction (PCR), and PCR products were observed in a DNA gel electrophoresis imager and photographed for analysis.

The qPCR methodology was conducted as previously described in He Y et al. [17], utilizing the same protocols and reagents for accurate gene expression analysis.

2.11. HDST assay

The living tumor tissues of the PDX models Nos. 1 and 2 were cut into $2 \times 2 \times 2$ mm^3 small blocks and placed in the culture wells of 96-well deep-hole plates (1.2 mL). Then, 100 μL of mixed special biohydrogel was added to each well. The mixtures were left for 30 min at room temperature. The experimental group was cultured with 700 μL of a tissue culture medium containing 0.5, 1, 2, 3, 4, or 5 mmol/L CGA. After 3 days, each supernatant was replaced with a fresh medium containing an equal amount of drug. Cell viability was detected by alamarBlue assay after 7 days of treatment. An alamarBlue solution was added to the complete medium, and the mixture was incubated for 16–20 h. ThermoScientific Fluoroskan FL (ThermoFisher Scientific, USA) was used to detect the fluorescence values of the solution at 544 nm excitation wavelength and 590 nm emission wavelength. All methods were performed according to the kit's instructions (Royo Biotech, Nanchang, China).

2.12. In vivo PDX model for drug efficacy evaluation

Drug administration was initiated when the tumor volume reached 30–80 mm^3. A total of 24 mice were equally randomized into the following groups: 1) blank control; 2) cisplatin, 0.625 mg/kg, intraperitoneal injection once a week; and 3) CGA, 6.25 mg/kg intraperitoneal injection daily. Body weight and subcutaneous tumor size were measured twice a week. The animals were euthanized by CO_2 asphyxiation 29 days after drug administration, and the tumors were excised and weighed.

TGI, which stands for Tumor Growth Inhibition, is calculated as the percentage reduction in tumor volume relative to the initial volume in the treatment group compared to the control group. The formula for TGI is given by:

$$\mathrm{TGI} = \left(1 - \left(\frac{Vt_{treatment}}{V0_{\mathrm{treatment}}}\right) \Big/ \left(\frac{\mathrm{Vt}_{\mathrm{control}}}{\mathrm{V0}_{\mathrm{control}}}\right)\right) \times 100\%$$

Where:

$Vt_{treatment}$ is the tumor volume at each measurement time point in the treatment group.

$V0_{treatment}$ is the initial tumor volume in the treatment group.

$Vt_{control}$ is the tumor volume at each measurement time point in the control group.

$V0_{control}$ is the initial tumor volume in the control group.

The benchmark for therapeutic efficacy, defined as a 30 % Tumor Growth Inhibition (TGI), is derived from the guidelines set forth

in the Histoculture Drug Response Assay (HDRA) documentation. This threshold indicates a significant impact on tumor growth suppression [18].

2.13. TUNEL assay

A TUNEL kit from Roche was used to assess apoptosis. The tissues were fixed in formalin, sliced into 4 μm-thick sections, and processed using xylene and graded ethanol. 4′,6-diamidino-2-phenylindole (DAPI) was used to counterstain the nucleus before mounting, and fluorescence microscopy was used for examination and image collection.

2.14. Immunofluorescence staining methodology

The immunofluorescence technique was performed following a standardized protocol, which includes slide baking, sequential deparaffinization with xylene and graded ethanol, antigen retrieval, and subsequent incubation with primary antibodies, followed by fluorescently labeled secondary antibodies. DAPI was used for nuclear counterstaining, and slides were mounted using an anti-fade reagent. The slides were then examined under a fluorescence microscope to visualize the specific antigen-antibody interactions.

2.15. Statistical analysis

Statistical analyses were performed using SPSS version 26.0 (IBM Corp., Armonk, NY, USA), and all figures were generated using Prism version 9.0 (NCH Corp., Santa Clara, CA, USA). The results were presented as means ± SD. Single-factor multilevel analysis was used to compare multiple groups, and the SNK method was used for comparing two groups. $p < 0.05$ indicated statistically significant difference.

3. Results

3.1. Established PDX model and validated consistency between the PDX models tissue and patient tissues

Two PDX models of tongue cancer were successfully constructed. The tissue morphology of a PDX model is similar to that of the patient with cancer according to the H&E staining results. The histopathological slides were reviewed by an experienced pathologist.

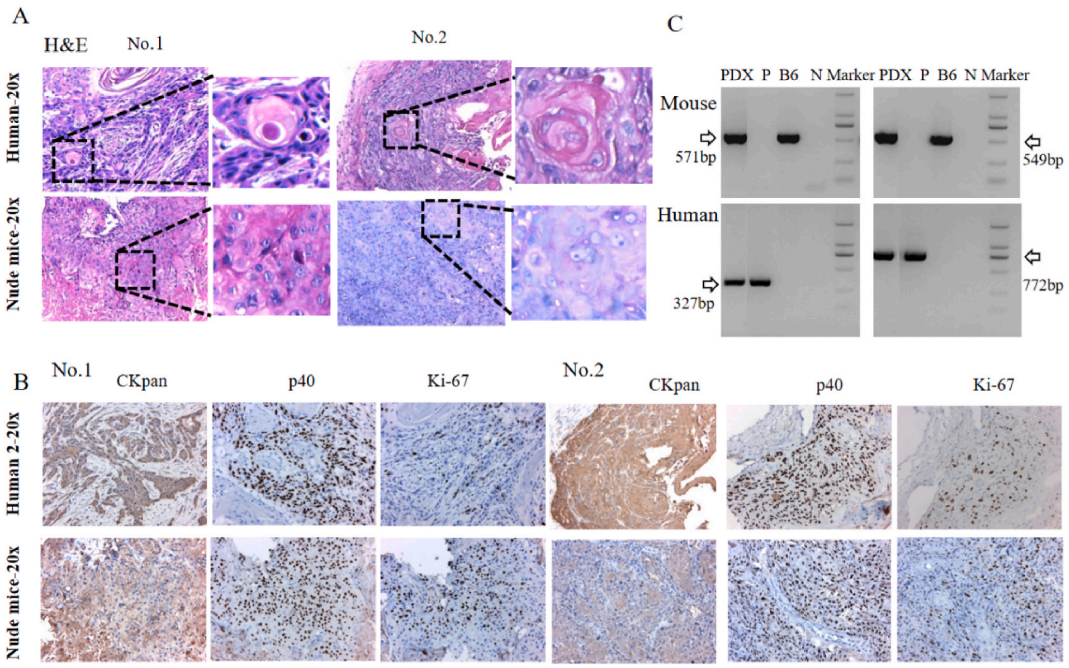

Fig. 1. H&E staining and IHC of PDX models tissue and patient tumor tissues.
(A) Tumors transplanted and grown in nude mice and tumors in the human tongue show tissue structural and cellular similarity, demonstrating the same molecular immunity. (B) CKpan and p40 are positive in the tumor cells of model Nos. 1 and 2 and Ki-67 (more than 5 % positive in both). (C) PCR identification of P5 generation mice (the full-length gel is shown in the Supplementary figure). Genomic DNA was extracted by PCR from established P0 and P5 tissues and analyzed by electrophoresis. The samples tested contained mouse- and human-derived genes. B6 was the P5 generation mouse.

The tumor cells in the human tongue and mice showed a markedly increased nucleoplasmic ratios and level of pathological nuclear division. The tumor cells in the human tongue were arranged in small nests, sheets, and cords and separated by fibers. In the mice, the tumor cells were arranged in sheets without fibrous separation (Fig. 1A). IHC staining of CKpan and P40 can aid in the diagnosis of squamous cell carcinoma of epithelial origin, whereas Ki-67 staining can assess cancer cell proliferation. The concordance between a PDX model tissue and the protein expression profile of a patient's tumor tissue was verified by evaluating the expression of CKpan, P40, and Ki-67. The results showed consistent protein expression patterns between the two samples (Fig. 1B). Genomic DNA was extracted from established PDX model tissues, amplified by PCR, and analyzed. The PDX model tumor tissue samples contained mouse and human target genes (Fig. 1C), indicating that the established PDX model was derived from the human tissues.

The result showed that the characteristics of the established PDX model tissue were consistent with the histological and IHC characteristics of the primary tumors.

3.2. CGA effectively inhibited the activity of tongue cancer cells in HDST

The effect of CGA on tongue canner in vitro was explored by testing the tumor activity of CGA against tongue carcinoma through HDST. A tumor growth inhibition rate greater than 30 % was considered effective [19,20]. The results showed that the inhibition rate of 2 mmol/L CGA for No.1 was 36.5 %, whereas the inhibition rate of 3 mmol/L CGA for No. 2 was 42.7 %. Tumor inhibition was concentration dependent within a certain range (Fig. 2).

3.3. CGA effectively inhibited tongue cancer growth in PDX model and had no significant side effects on mice

In the PDX models, the cisplatin and CGA groups demonstrated effective inhibitory effects on tumor growth after 29 days of treatment. (Fig. 3A–F). After a 29-day observation period, the tumor volumes for the control, CGA, and cisplatin groups in experiment No. 1 were recorded as 427.64, 263.72, and 73.14 mm^3, respectively. In experiment No. 2, these values were 587.74, 423.52, and 220.40 mm^3, respectively (Fig. 3B–G). The TGI for the cisplatin and CGA groups were 84.61 % and 38.79 % in experiment No. 1, and 72.63 % and 41.54 % in experiment No. 2, respectively (Fig. 3C–H). In experiment No. 1, the mean tumor weights for the control, CGA, and cisplatin groups were recorded as 0.36 g, 0.055 g, and 0.22 g, respectively (as depicted in Fig. 3D). Similarly, in experiment No. 2, these values were 0.54 g for the control group, 0.15 g for the CGA group, and 0.32 g for the cisplatin group (illustrated in Fig. 3I). In the conducted experiments, the mean tumor weights in the CGA group showed a decreasing trend compared to the Control group, with values of 0.055 g and 0.15 g in experiments No. 1 and No. 2, respectively, as opposed to the control group's 0.36 g and 0.54 g.

Mice with severe immune deficiency typically exhibit a significant reduction in T cells and natural killer (NK) cells, as well as impaired neutrophil function and a decrease in lymphocytes [21]. These characteristics are consistent with the immune-deficient mouse model used in our study. In our experimental observations, we noted a significant reduction in tumor cell size and observed extensive areas of necrosis, including fibrinoid necrosis and apoptosis, characterized by evident nuclear fragmentation. Within these necrotic areas, we identified pink collagen deposits, indicating the transformation of fibrotic tissue into collagen. Notably, in the CGA group, we observed more pronounced hyaline degeneration, with further reduction in tumor cells and nuclear atypia (Fig. 3E–J).

In our experiments, we noted a significant observation regarding the survival of mice across different treatment groups. Specifically, in the cisplatin group, three mice succumbed in each instance, whereas only one mouse in the control group died. Notably, no fatalities were recorded in the group treated with CGA. To further evaluate the safety of CGA treatment, we performed H&E staining to scrutinize histopathological changes in vital organs, including the heart, liver, spleen, lungs, and kidneys. Our analysis revealed no significant signs of toxicity in these organs (Fig. 4). Additionally, when comparing the body weight changes, mice in groups No.1 and No.2, which were administered cisplatin, exhibited a significant weight loss compared to the CGA-treated groups (Fig. 5). These findings collectively suggest that CGA demonstrates a potentially more favorable safety profile than cisplatin in our experimental conditions.

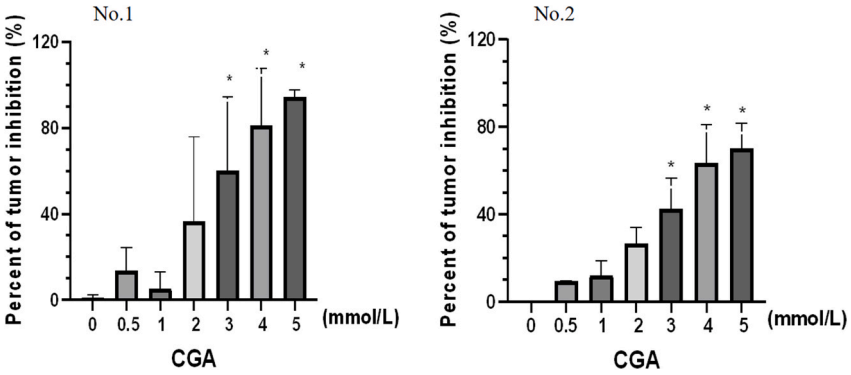

Fig. 2. AlamarBlue staining of tongue cancer tissue. The viability of HDST cells subjected to CGA treatment was assayed by alamarBlue staining. Statistical data showed that 3, 4, and 5 mmol/L CGA inhibited tongue cancer tissues (*, $p < 0.05$).

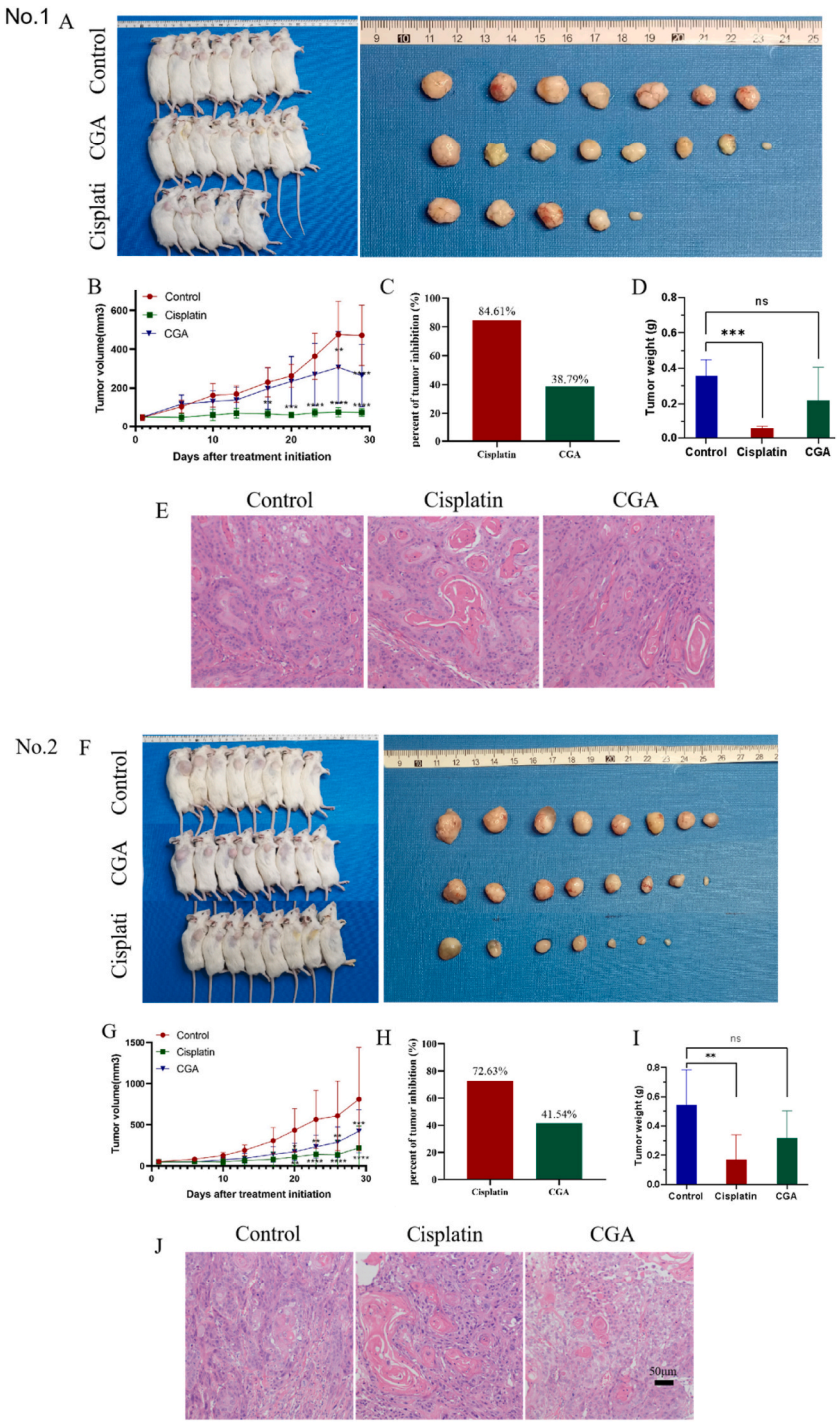

Fig. 3. CGA inhibited tongue cancer in vivo effectively. (A, F) The PDX model showed that CGA inhibited tongue cancer in Nos. 1 and 2. (B, C, G, H) CGA inhibited the tumor volume and tumor weight. (D, I) The tumor inhibition rates of CGA in Nos. 1 and 2 were 38.79 % and 41.54 %, respectively. (E, J) Tissue fibrosis and inflammatory cell infiltration in the CGA and cisplatin groups (*, $p < 0.05$).The original data are shown in the supplementary table.

3.4. CGA inhibited angiogenesis and induced cell apoptosis

In the course of our investigation, we observed that both CGA and cisplatin exerted inhibitory effects on angiogenesis and induced cellular apoptosis. Specifically, the expression levels of CD31, a quintessential marker for angiogenesis, and KI-67, a proliferation-

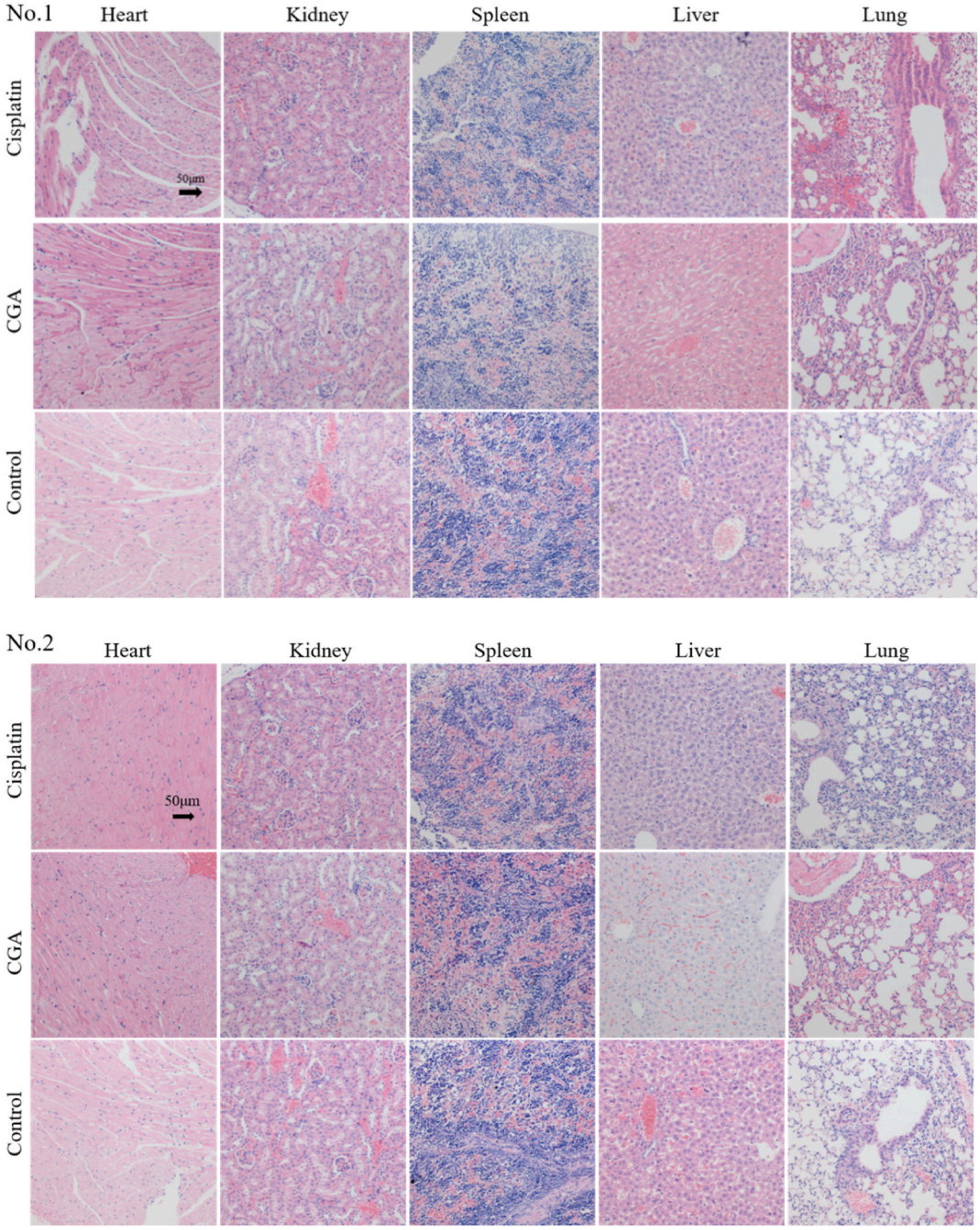

Fig. 4. Heart, liver, spleen, lung, and kidney were sectioned and stained with H&E after CGA and cisplatin treatments.

associated marker, were significantly reduced in response to treatment with CGA and, to a greater extent, with cisplatin (Fig. 6). This suggests that while CGA effectively suppresses the vascularization supporting tumor growth, cisplatin demonstrates a more pronounced impact on these processes. Furthermore, the TUNEL assay, a standard method for detecting apoptotic cells, revealed an increase in apoptosis in both treatment groups. Notably, the CGA treatment group exhibited a more substantial enhancement in TUNEL-positive cells compared to the cisplatin group, indicating a heightened induction of apoptosis by CGA (Fig. 7). These results collectively suggest that CGA possesses the potential to elicit a robust apoptotic response in tumor cells, which may contribute to its anti-tumor activity.

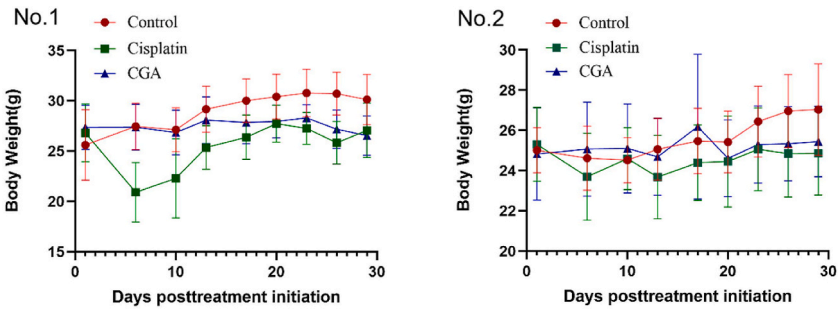

Fig. 5. Body weight of mice post-treatment.

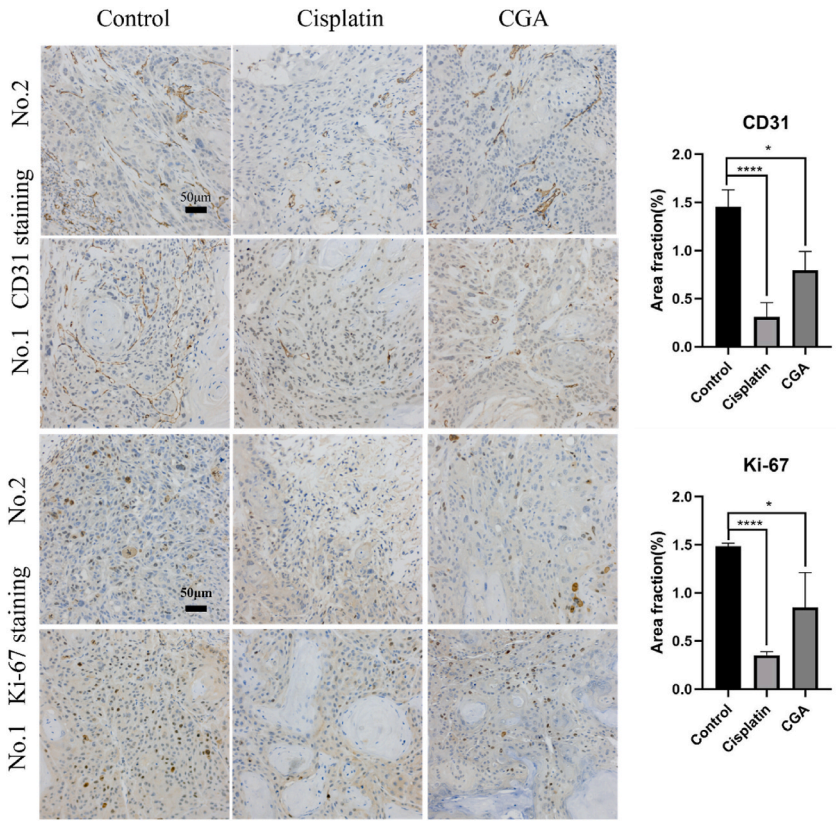

Fig. 6. CGA affected the expression of CD31 and Ki-67. CD31-positive blood vessels were reduced, and Ki-67-positive cell rate was downregulated after CGA treatment (Brown-stained nuclei represent positive staining; *, $p < 0.05$). (For interpretation of the references to color in this figure legend, the reader is referred to the Web version of this article.)

3.5. Network pharmacology analysis of CGA targets and pathways in tongue cancer

Potential targets of CGA were predicted using the Swiss Target Prediction and BATMAN-TCM 2.0 databases, and 232 valid targets were identified after excluding ineffective components. Concurrently, 1481 tongue cancer-related targets were filtered from the Genecards, and OMIM databases. A Venn diagram analysis revealed 58 common targets between CGA and tongue cancer (Fig. 8A). Subsequently, a protein-protein interaction (PPI) network analysis was conducted on these targets using the STRING database, which suggested that genes such as AKT1, EGFR, CASP3, MMP9, and ESR1 might be key targets for CGA in the treatment of tongue cancer (Fig. 8B and C).

Furthermore, an intersection approach was employed to identify disease-related targets from the drug data, which were then analyzed using Cytoscape 3.7.2 (Fig. 8D). The Gene Ontology (GO) enrichment analysis yielded a total of 1908 results, including 1701 biological process (BP) terms primarily peptidyl-tyrosine phosphorylation, peptidyl-tyrosine modification, and protein autophosphorylation; 44 cellular component (CC) terms related to membrane raft, membrane microdomain, and membrane region; and 163

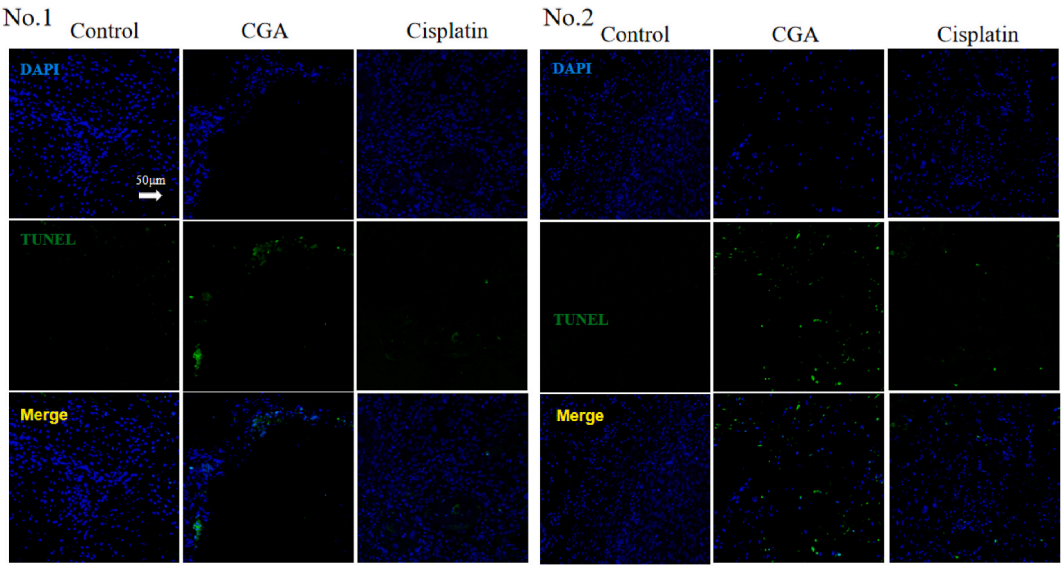

Fig. 7. CGA treatment induced cell apoptosis as detected by the TUNEL assay (blue-green-stained nuclei represent positive staining). All cell nuclei were stained blue by DAPI fluorescent staining to prevent interference from impurities. Apoptotic cell nuclei were stained green by Fluorescein isothiocyanate (FITC) fluorescent staining. The merged image represented the overlapping of the differently stained nuclei, and the blue-green nuclei represented the apoptotic nuclei. (For interpretation of the references to color in this figure legend, the reader is referred to the Web version of this article.)

molecular function (MF) terms involving protein tyrosine kinase activity, transmembrane receptor protein tyrosine kinase activity, and transmembrane receptor protein kinase activity. The Kyoto Encyclopedia of Genes and Genomes (KEGG) enrichment analysis identified 136 pathways, predominantly involving the Lipid and atherosclerosis and PI3K-Akt signaling pathway, suggesting that CGA may intervene in tongue cancer through these pathways ($P < 0.05$) (Fig. 9).

3.6. CGA targets EGFR-AKT-MMP9 in tongue cancer

Through network pharmacology analysis, we have delineated the molecular mechanism by which CGA exerts its inhibitory effects on tongue cancer. Activated by EGF, EGFR triggers pathways that activate AKT1, which in turn upregulates MMP9, an enzyme aiding in tissue repair, blood vessel growth, and cancer spread [22]. While it is mainly active outside the cell, MMP9 can also be found within the cytoplasmic compartment after being secreted by the cell. Experimental results indicate that in the CGA-treated group, the fluorescence intensity of EGFR, AKT, and MMP9 was significantly reduced compared to the control group (Fig. 10). This suggests that CGA may exert its anti-oral cancer effect by modulating this signaling pathway.

4. Discussion

In this study, two PDX models of tongue cancer were successfully constructed. Pathological examination showed that the PDX models and patients' tumor tissues displayed increased nuclear-to-cytoplasmic ratios and frequency of pathologic mitosis. The morphology of the PDX models tumor tissues closely resembled that of the patients'. Moreover, the two PDX models were considered tumors of the squamous epithelium. P40 was considered the most specific and sensitive marker of squamous epithelium [23]. CKpan is used to determine whether a tumor is of epithelial origin, and Ki-67 is a proliferating cell-associated nuclear antigen. The proliferation rates and malignancy of tumor cells increases with its positive expression level. In terms of morphology and protein expression pattern, the PDX models are similar to the patients' tumor tissues.

A team in Korea has constructed a sample bank of 15 head and neck squamous cell carcinomas [24], including tongue cancer [25]. The increasing demand for PDX models as tools for drug efficacy evaluation underscores the importance of a large PDX library, and a large repository of PDX models provides a valuable resource for innovation and drug discovery [26]. Therefore, our PDX model is an important tool for tongue cancer research. Although PDX models have been developed for tongue cancer, they are limited by their high costs and long preparation times. HDST is a novel method that was independently developed by our team. According to the mechanobiology theory, the growth characteristics of tumor cells in matrices of different hardness vary, including their responses to drugs [27]. A tumor tissue is encapsulated by a hydrogel, which provides lateral pressure and thereby effectively simulates a tumor tissue environment in the body. Compared with other screening methods, HDST can effectively simulate the tumor growth environment, has a convenient operation, and produces highly consistent results in clinical practice.

The HDST results assay indicated that 3 mmol/L CGA inhibited tongue cancer effectively, and the inhibition rates were as high as 72%–91 %. The inhibitory effect was concentration dependent within a certain range. Yamagata [28] utilized only 30 or 50 μmol/L

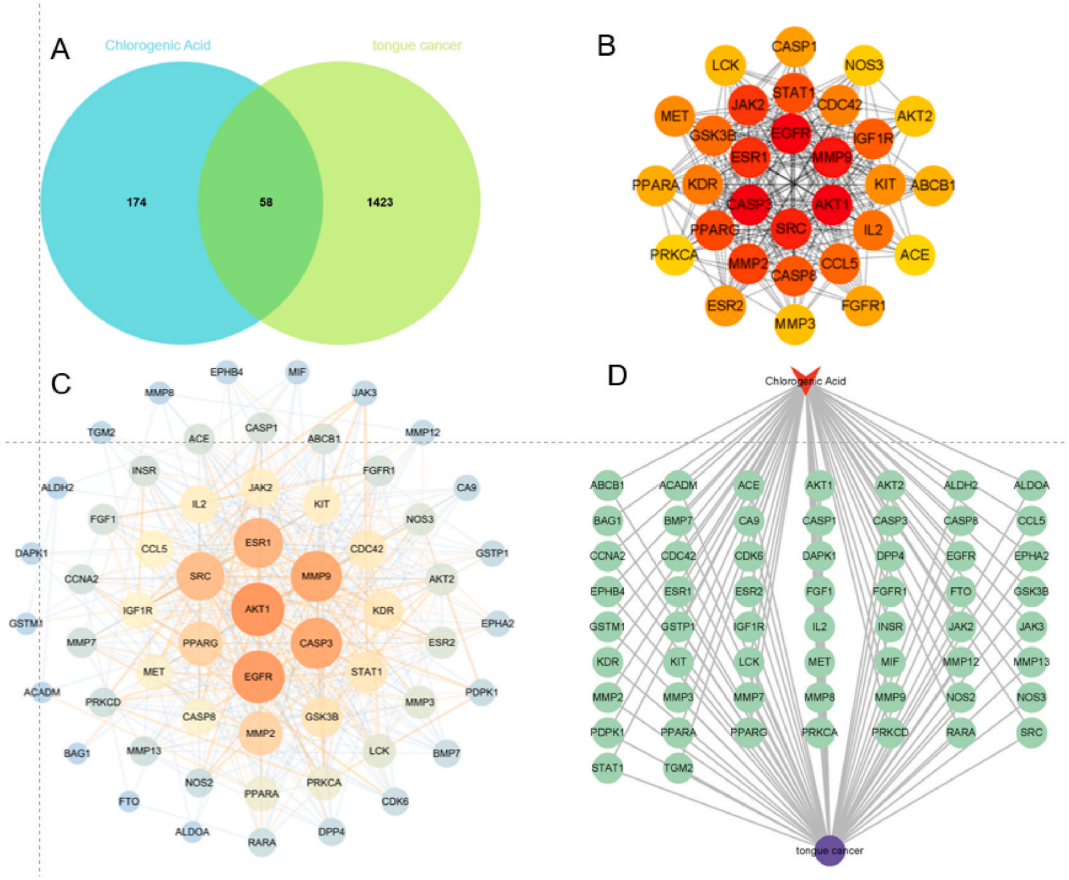

Fig. 8. Network Pharmacology Analysis. (A) Comparative Venn diagram of molecular targets for CGA and Tongue Cancer. (B) Network analysis of hub genes common to CGA and tongue cancer. (C) PPI network of hub proteins associated with CGA and tongue cancer. (D) Molecular interaction network of CGA and tongue cancer-related genes.

CGA to treat cancer cells, however, the concentration of CGA in our experiment was higer. Given that tumor tissue blocks are coated with hydrogels in HDST, drugs need to pass through the hydrogels before they can infiltrate the tissues and treat the cells.

Several clinical trials on CGA are already in progress [29]. Our results were consistent with those of previous reports, which showed that CGA plays an important role in the regulation of tumor cell proliferation and apoptosis [30–32]. The present experiment demonstrated that CGA has a good inhibitory effect on tongue cancer tumor tissues. This effect was confirmed in the PDX models, indicating its good prospects for the clinical treatment of tongue cancer.

CD31, a platelet–endothelial cell adhesion molecule, is primarily used in assessing tumor angiogenesis [33]. Tumor angiogenesis is essential for the continued survival and development of tumor cells and plays an important role in the growth, invasion, and metastasis of tumor cells [34]. In this study, the number of CD31-positive microvessels decreased in the CGA group, indicating that CGA can inhibit angiogenesis in tongue cancer. Studies have shown that CGA inhibits angiogenesis by inhibiting the HIF-1α/AKT pathway and thereby suppresses the growth of lung cancer [35]. It can affect the expression of apoptosis-related genes, such as *BCL2*, *BAX*, and *CASP3*, and contribute to antitumor effects [36]. In our study, Ki-67-positive cell rate decreased, and the TUNEL (+) cell rate increased. These results indicated that CGA inhibits tongue cancer through multiple pathways, particularly by suppressing the proliferation of cancer cells and promoting apoptosis while inhibiting angiogenesis.

Additionally, our study indicates that compared to cisplatin, CGA induces a higher level of apoptosis, as evidenced by an enhanced green signal. Cisplatin, a widely utilized clinical chemotherapeutic agent, primarily induces necrosis by causing DNA damage, leading to rapid cell death, with a relatively minor induction of apoptosis [37]. In contrast, CGA exerts a milder effect, predominantly promoting apoptosis. This distinction suggests that CGA may be suitable for therapeutic scenarios where the induction of apoptosis is desired, such as in the elimination of cancer stem cells or the reduction of tumor growth, while minimizing collateral damage to surrounding tissues.

To elucidate the specific mechanisms of CGA's anti-apoptotic and angiogenesis-inhibitory actions, we utilized single-color immunofluorescence to examine the expression of EGFR, AKT, and MMP9. EGFR, a transmembrane receptor tyrosine kinase, plays a pivotal role in cell proliferation, differentiation, migration, and survival. Its activation is typically induced by the binding of its ligands, such as epidermal growth factor (EGF). Upon ligand binding, EGFR undergoes dimerization and autophosphorylation,

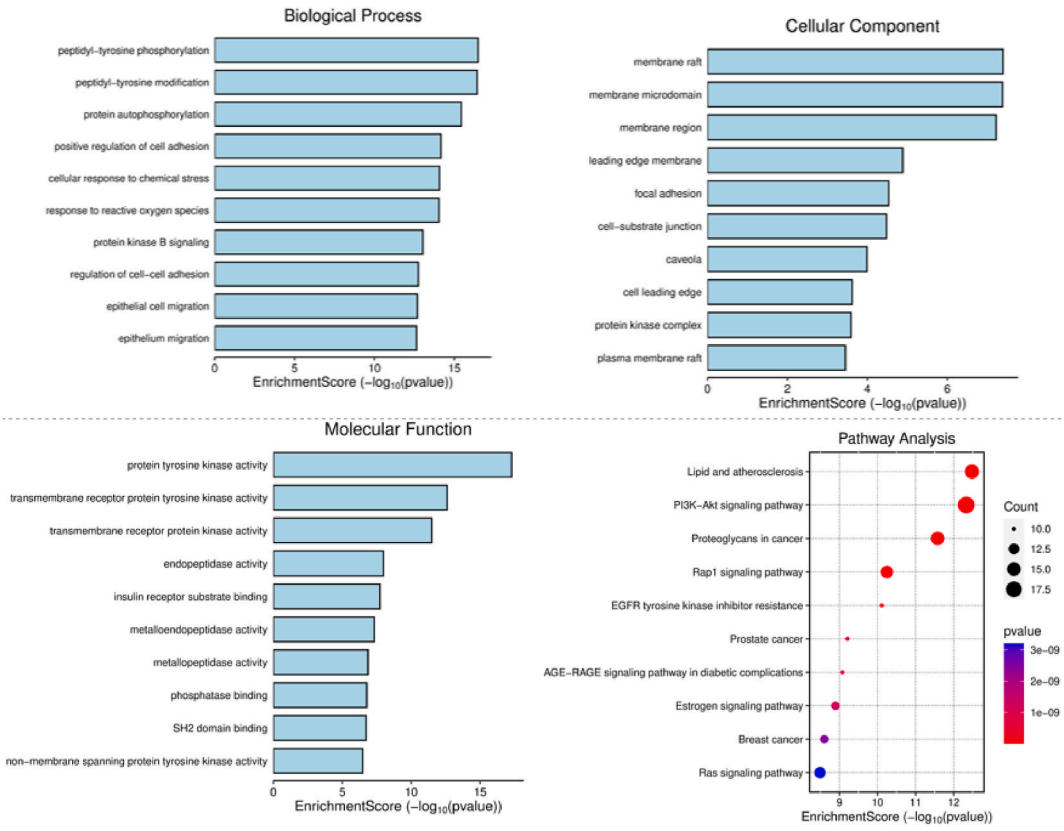

Fig. 9. Gene Ontology (GO) and KEGG Pathway analysis enrichment scores for CGA-related tongue cancer Genes.

activating its kinase activity and initiating downstream signal transduction [38]. AKT, a serine/threonine kinase, is implicated in the regulation of cell survival, proliferation, metabolism, and angiogenesis. Once EGFR is activated, it can activate AKT through the PI3K/PDK1 pathway [39]. MMP9, a zinc-dependent endopeptidase, is capable of degrading the extracellular matrix, thereby promoting tumor invasion and angiogenesis [40]. The expression and activity of MMP9 are regulated by various factors, including the AKT and ERK signaling pathways. The EGFR-ERK/AKT-MMP9 signaling pathway, while crucial in normal physiological processes, may be aberrantly activated during tumorigenesis, facilitating the proliferation, survival, invasion, and angiogenesis of tumor cells, and thus accelerating tumor progression [41]. Studies have indicated that Akt and MAPK mediate the signaling of HRG-β1 to MMP-9, affecting the invasion and metastasis of breast cancer [42]. MMP9 can promote angiogenesis, and our experimental results observed a significant decrease in CD31, suggesting that CGA may exert its anti-oral cancer effects through the EGFR-AKT-MMP9 signaling pathway, with the ERK1/2 pathway potentially regulating this process.

CGA, a natural compound found in various foods and traditional Chinese medicine, has shown promising inhibitory effects on tumor growth in vitro, outperforming cisplatin in inducing apoptosis and inhibiting angiogenesis. However, its in vivo antitumor efficacy against tongue cancer, while present, is less pronounced compared to cisplatin. CGA reduced the tumor volume and weight in mice by 38.79 % in experiment No.1 and 41.54 % in No.2, relative to the control group, yet these effects were not as pronounced as those observed in the cisplatin group. The observed reduction in tumor growth did not achieve statistical significance compare to the control group, which is likely attributed to a combination of factors. Primarily, the small sample size (n) may have constrained the study's power to detect a genuine effect, and secondarily, the fixed threshold applied in the analysis could have contributed to the non-significance of the results. In the cisplatin group, where a rapid cytotoxic impact was noted, albeit with the cost of three mice deaths in No.1. The body weight of mice treated with CGA was higher compared to those treated with cisplatin. This finding suggests that CGA may have a better safety profile in terms of body weight maintenance. Regarding cisplatin group, we observed that three mice in each group passed away following treatment, indicating a significant level of toxicity associated with cisplatin. This observation is consistent with the known side effects of cisplatin and highlights the need for alternative treatments with reduced toxicity.

CGA is recognized for its efficacy and safety, with low toxicity and minimal side effects, making it a viable treatment option for individuals with weakened health conditions [43,44]. Despite the less pronounced in vivo effects, CGA's role in the clinical treatment of tongue cancer should not be overlooked, as it has shown positive effects on various cancer cells, including glioblastoma, lung cancer, and ovarian cancer cells [45–47]. Further research is necessary to explore the related genes, proteins, and molecular mechanisms underlying CGA's action in tongue cancer, with the aim to optimize its therapeutic potential and reconcile the observed differences in efficacy between in vitro and in vivo conditions.

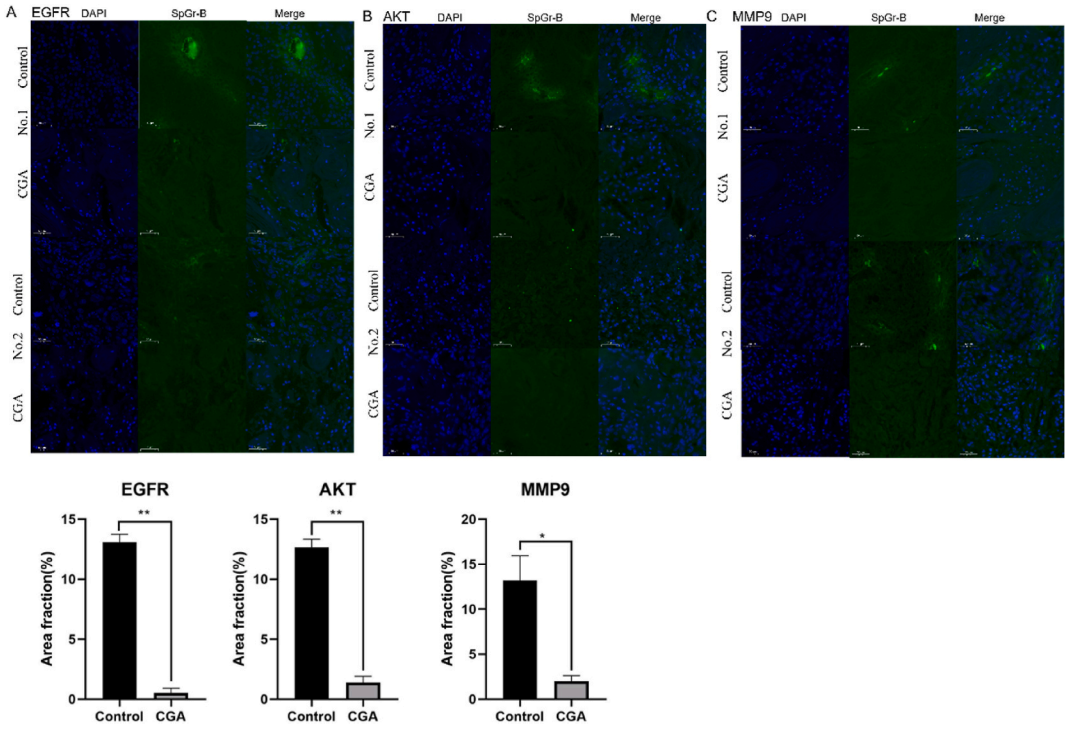

Fig. 10. Downregulation of EGFR, AKT, and MMP9 Protein Expression Following CGA Treatment. In the monochrome immunofluorescence assay, cell nuclei were stained blue-green to identify target antigens. DAPI was used for nuclear counterstaining to enhance contrast against the background. The cytoplasmic proteins were visualized with the SpGr-B stain, which fluoresces green. The merged image illustrates the cellular localization of the proteins, with nuclei in blue and cytoplasmic proteins in green. (For interpretation of the references to color in this figure legend, the reader is referred to the Web version of this article.)

5. Conclusions

The present experiment reports the successful establishment of PDX models of two cases of tongue cancer and reveals the inhibitory effects of CGA in vivo and in vitro. The underlying mechanism of its action can be attributed to its effects on angiogenesis inhibition and cell apoptosis.

Consent for publication

All the authors read and agreed to publish this article.

Funding

This work was funded by the Natural Foundation of Jiangxi Province (No. 20192BCD40003 to YQ He), and Jiangxi Provincial Science and Technology Department Project Natural Science Foundation (No. 20202BABL206067 to XP Hu).

Availability of data and materials

All the data analysis results obtained during this study are included in the manuscript. The original contributions presented in this study can be obtained upon request by contacting the corresponding author via email.

Ethics approval and consent to participate

Animal ethics: The experiment protocol for the mice used for the PDX models was approved by the IACUC of Royo Biotech Co., Ltd. (RYE: 2020021701, Nanchang, China). The animal transport, husbandry, and experimental procedures were performed in accordance with the national legislation (SN/T 3986-2014) on the protection of animals used for scientific or educational purposes. The animals were purchased from GemPharmatech Co., Ltd., Jiangsu, China. After surgical operations and experiment, the animals were euthanized by CO_2 asphyxiation. All methods are reported in accordance with ARRIVE guidelines for the reporting of animal experiments.

Human ethics: This experiment was approved by the ethics committees of the Affiliated Stomatological Hospital of Nanchang

University (Permit No. 2021016). All patients provided informed consent and signed relevant informed consent forms before surgery. The personal privacy information of all patients was strictly protected throughout the research process, and all data were handled anonymously. This experiment was performed according to the ethical principles of the Declaration of Helsinki.

Ethics Statement

This study was conducted in accordance with the principles of the Declaration of Helsinki. All animal studies were approved by the IACUC of Nanchang Royo Biotech Co., Ltd. (Permit No. RYE2020021701).

The patients signed the informed consent form, and sample collection was approved by the Affiliated Stomatological Hospital of Nanchang University (Permit No. 2021016).

Informed consent was obtained from all participants before enrolment into the study. The privacy of all participants was strictly protected throughout the study, and personal information was kept confidential. All data were collected and analyzed carefully, and the results presented in this article are truthful, accurate, and reliable.

CRediT authorship contribution statement

Jia Zhu: Formal analysis, Data curation. **Jiaqi Mei:** Writing – original draft. **Yuanqiao He:** Supervision. **Yan Zou:** Formal analysis, Data curation. **Xiaoping Hu:** Supervision, Resources, Project administration, Conceptualization.

Declaration of competing interest

The authors declare that they have no known competing financial interests or personal relationships that could have appeared to influence the work reported in this paper.

Acknowledgments

We thank Nanchang Royo Biotechnology for the technical assistance and instrument support of Jiangxi Provincial Key Laboratory of Laboratory Animals.

We thank pathologist Liqing Wu for the production and identification of the H&E sections.

Appendix A. Supplementary data

Supplementary data to this article can be found online at https://doi.org/10.1016/j.heliyon.2024.e37523.

References

[1] R. Li, W.M. Koch, C. Fakhry, C.G. Gourin, Distinct epidemiologic characteristics of oral tongue cancer patients, Otolaryngol. Head Neck Surg. 148 (5) (2013) 792–796.
[2] D.K. Zanoni, P.H. Montero, J.C. Migliacci, J.P. Shah, R.J. Wong, I. Ganly, et al., Survival outcomes after treatment of cancer of the oral cavity (1985-2015), Oral, Oncol. 90 (2019) 115–121.
[3] A. Parmar, M. Macluskey, N.Mc Goldrick, D.I. Conway, A.M. Glenny, J.E. Clarkson, et al., Interventions for the treatment of oral cavity and oropharyngeal cancer: chemotherapy, Cochrane Database Syst. Rev. 12 (12) (2021) CD006386.
[4] N. Vasan, J. Baselga, D.M. Hyman, A view on drug resistance in cancer, Nature 575 (7782) (2019) 299–309.
[5] A. Almangush, I.O. Bello, H. Keski-Säntti, L.K. Mäkinen, J.H. Kauppila, M. Pukkila, et al., Depth of invasion, tumor budding, and worst pattern of invasion: prognostic indicators in early-stage oral tongue cancer, Head, Neck. 36 (6) (2014) 811–818.
[6] I.O. Bello, Y. Soini, T. Salo, Prognostic evaluation of oral tongue cancer: means, markers and perspectives (I), Oral Oncol. 46 (9) (2010) 630–635.
[7] M. Ibarrola-Villava, A. Cervantes, A. Bardelli, Preclinical models for precision oncology, Biochim. Biophys. Acta. Rev. Cancer. 1870 (2) (2018) 239–246.
[8] S.Y. Cho, W. Kang, J.Y. Han, S. Min, J. Kang, A. Lee, et al., An Integrative approach to precision cancer medicine using patient-derived xenografts, Mol. Cells. 39 (2) (2016) 77–86.
[9] J.J. Tentler, A.C. Tan, C.D. Weekes, A. Jimeno, S. Leong, T.M. Pitts, et al., Patient-derived tumour xenografts as models for oncology drug development, Nat. Rev. Clin. Oncol. 9 (6) (2012) 338–350.
[10] Y. He, J. Mei, H. Hao, F. Liu, Y. Yi, C. Hu, et al., Selinexor demonstrates anti-tumor efficacy in paired patient-derived xenograft models and hydrogel-embedded histoculture drug sensitivity test of penile cancer, J. Cancer Res. Clin. Oncol. 149 (10) (2023) 6931–6941.
[11] H. Lu, Z. Tian, Y. Cui, Z. Liu, X. Ma, A comprehensive review of the dietary sources, processing effects, bioavailability, beneficial properties, mechanisms of action, and future directions, Compr. Rev. Food Sci. Food Saf. 19 (6) (2020) 3130–3158.
[12] A. Gupta, A.G. Atanasov, Y. Li, N. Kumar, A. Bishayee, Chlorogenic acid for cancer prevention and therapy: current status on efficacy and mechanisms of action, Pharmacol. Res. 186 (2022) 106505.
[13] L. Wang, H. Du, P. Chen, Chlorogenic acid inhibits the proliferation of human lung cancer A549 cell lines by targeting annexin A2 in vitro and in vivo, Biomed. Pharmacother. 131 (2020) 110673.
[14] K. Yagasaki, Y. Miura, R. Okauchi, T. Furuse, Inhibitory effects of chlorogenic acid and its related compounds on the invasion of hepatoma cells in culture, Cytotechnology 33 (1–3) (2020) 229–235.
[15] Z. Changizi, A. Moslehi, A.H. Rohani, A. Eidi, Chlorogenic acid induces 4T1 breast cancer tumor's apoptosis via p53, Bax, Bcl-2, and caspase-3 signaling pathways in BALB/c mice, J. Biochem. Mol. Toxicol. 35 (2) (2021) e22642.
[16] A. Salzillo, A. Ragone, A. Spina, S. Naviglio, L. Sapio, Chlorogenic acid enhances doxorubicin-mediated cytotoxic effect in osteosarcoma cells, Int. J. Mol. Sci. 22 (16) (2021) 8586.

[17] Y. He, J. Mei, H. Hao, F. Liu, Y. Yi, C. Hu, F. Zou, X. Lu, Selinexor demonstrates anti-tumor efficacy in paired patient-derived xenograft models and hydrogel-embedded histoculture drug sensitivity test of penile cancer, J. Cancer Res. Clin. Oncol. 149 (10) (2023) 6931–6941.
[18] J. Lee, J.M. Kim, Y.H. Lee, G.O. Chong, D.G. Hong, Applicability of the histoculture drug response assay to predict platinum sensitivity and prognosis in ovarian cancer, Anticancer. Research. 41 (12) (2021) 6287–6292.
[19] T. Kubota, N. Sasano, O. Abe, I. Nakao, E. Kawamura, T. Saito, M. Endo, K. Kimura, H. Demura, H. Sasano, et al., Potential of the histoculture drug-response assay to contribute to cancer patient survival, Clin. Cancer Res. 1 (12) (1995) 1537–1543.
[20] Q. Rao, Y. Wei, S. Lin, Y. Peng, R. Lin, Y. He, et al., Effect of HDST technology in neoadjuvant chemotherapy for ovarian cancer, Journal. Of. Sun. Yat.-sen. University. (Medical. Sciences) 41 (5) (2020) 795–801.
[21] M.A. Grundy, C.L. Sentman, Immunodeficient mice have elevated numbers of NK cells in non-lymphoid tissues, Exp. Cell Res. 312 (19) (2006) 3920–3926.
[22] H. Huang, Matrix metalloproteinase-9 (MMP-9) as a cancer biomarker and MMP-9 biosensors: recent advances, Sensors 18 (10) (2018) 3249.
[23] X. Jiang, J. Wang, X. Deng, F. Xiong, S. Zhang, Z. Gong, et al., The role of microenvironment in tumor angiogenesis, J. Exp. Clin. Cancer Res. 39 (1) (2020) 204.
[24] H.N. Kang, J.H. Kim, A.Y. Park, J.W. Choi, S.M. Lim, J. Kim, et al., Establishment and characterization of patient-derived xenografts as paraclinical models for head and neck cancer, BMC Cancer 20 (1) (2020) 316.
[25] K. Hasegawa, S. Fujii, K.J. Kurppa, T. Maehara, K. Oobu, S. Nakamura, et al., Clear cell squamous cell carcinoma of the tongue exhibits characteristics as an undifferentiated squamous cell carcinoma, Pathol. Res. Pract. 235 (2022) 153909.
[26] A. Collins, G.J. Miles, J. Wood, M. MacFarlane, C. Pritchard, E. Moss, Patient-derived explants, xenografts and organoids: 3-dimensional patient-relevant pre-clinical models in endometrial cancer, Gynecol. Oncol. 156 (1) (2020) 251–259.
[27] L. Zhu, X. Fan, B. Wang, L. Liu, X. Yan, L. Zhou, Biomechanically primed liver microtumor array as a high-throughput mechanopharmacological screening platform for stroma-reprogrammed combinatorial therapy, Biomaterials 124 (2017) 12–24.
[28] K. Yamagata, Y. Izawa, D. Onodera, D. Onodera, M. Tagami, Chlorogenic acid regulates apoptosis and stem cell marker-related gene expression in A549 human lung cancer cells, Mol. Cell. Biochem. 441 (2018) 9–19.
[29] T. Ren, Y. Wang, C. Wang, M. Zhang, W. Huang, J. Jiang, et al., Isolation and identification of human metabolites from a novel anti-tumor candidate drug 5-chlorogenic acid injection by HPLC-HRMS/MSn and HPLC-SPE-NMR, Anal. Bioanal. Chem. 409 (30) (2017) 703–7048.
[30] E.O. Nwafor, P. Lu, Y. Zhang, R. Liu, H. Peng, B. Xing, et al., Chlorogenic acid: potential source of natural drugs for the therapeutics of fibrosis and cancer, Transl. Oncol. 15 (1) (2022) 101294.
[31] Li Wang, P. Zou, X. Gao, H. Meng, Y. He, X. Liu, et al., Chlorogenic acid regulates the proliferation and migration of high-grade serous ovarian cancer cells through modulating the miR199a5p/DDR1 axis, Acta Biochim. Pol. 69 (4) (2022) 855–864.
[32] A. Zeng, X. Liang, S. Zhu, C. Liu, S. Wang, Q. Zhang, et al., Chlorogenic acid induces apoptosis, inhibits metastasis and improves antitumor immunity in breast cancer via the NF-κB signaling pathway, Oncol, Rep. 45 (2) (2021) 717–727.
[33] C.C. Figueiredo, N.B. Pereira, L.X. Pereira, L.A.M. Oliveira, P.P. Campos, S.P. Andrade, Double immunofluorescence labeling for CD31 and CD105 as a marker for polyether polyurethane-induced angiogenesis in mice, Histol. Histopathol. 34 (3) (2019) 257–264.
[34] S.M. Weis, D.A. Cheresh, Tumor angiogenesis: molecular pathways and therapeutic targets, Nat. Med. 17 (11) (2011) 1359–1370.
[35] J.J. Park, S.J. Hwang, J.H. Park, H.J. Lee, Chlorogenic acid inhibits hypoxia-induced angiogenesis via down-regulation of the HIF-1α/AKT pathway, Cell. Oncol. 38 (2) (2015) 111–118.
[36] R. Rashidi, R. Rezaee, A. Shakeri, A.W. Hayes, G. Karimi, A review of the protective effects of chlorogenic acid against different chemicals, J. Food Biochem. 46 (9) (2022) e14254.
[37] R.C. Kiss, F. Xia, S. Acklin, Targeting DNA damage response and repair to enhance therapeutic index in cisplatin-based cancer treatment, Int. J. Mol. Sci. 22 (15) (2021) 8199.
[38] B.R. Voldborg, L. Damstrup, M. Spang-Thomsen, H.S. Poulsen, Epidermal growth factor receptor (EGFR) and EGFR mutations, function and possible role in clinical trials, Ann. Oncol. 8 (12) (1997) 1197–1206.
[39] S. Revathidevi, A.K. Munirajan, Akt in cancer: mediator and more, Semin. Cancer Biol. 59 (2019) 80–91.
[40] M. De Palma, D. Biziato, T.V. Petrova, Microenvironmental regulation of tumour angiogenesis, Nat. Rev. Cancer 17 (8) (2017) 457–474.
[41] L. Li, P. Fan, H. Chou, J. Li, K. Wang, H. Li, Herbacetin suppressed MMP9 mediated angiogenesis of malignant melanoma through blocking EGFR-ERK/AKT signaling pathway, Biochimie 162 (2019) 198–207.
[42] S.J. Cho, M.J. Chae, B.K. Shin, H.K. Kim, A. Kim, Akt- and MAPK-mediated activation and secretion of MMP-9 into stroma in breast cancer cells upon heregulin treatment, Mol. Med. Rep. 1 (1) (2008) 83–88.
[43] Y. Yu, Z. Zhang, C. Chang, Chlorogenic acid intake guidance: sources, health benefits, and safety, Asia Pac. J. Clin. Nutr. 31 (4) (2022) 602–610.
[44] H. Lu, Z. Tian, Y. Cui, Z. Liu, X. Ma, Chlorogenic acid: a comprehensive review of the dietary sources, processing effects, bioavailability, beneficial properties, mechanisms of action, and future directions, Compr. Rev. Food Sci. Food Saf. 19 (6) (2020) 3130–3158.
[45] N. Xue, Q. Zhou, M. Ji, J. Jin, F. Lai, J. Chen, et al., Chlorogenic acid inhibits glioblastoma growth through repolarizating macrophage from M2 to M1 phenotype, Sci. Rep. 7 (2017) 39011.
[46] J. Tai, S. Cheung, E. Chan, D. Hasman, Antiproliferation effect of commercially brewed coffees on human ovarian cancer cells in vitro, Nutr. Cancer 62 (8) (2010) 1044–1057.
[47] P.H. Hsu, W.H. Chen, C. Juan-Lu, S.C. Hsieh, S.C. Lin, R.T. Mai, et al., Hesperidin and chlorogenic acid synergistically inhibit the growth of breast cancer cells via estrogen receptor/mitochondrial pathway, Life 11 (9) (2021) 950.